Interannual Variability of the Subsurface High Salinity Tongue South of the Equator at 165°E*

WILLIAM S. KESSLER

NOAA/Pacific Marine Environmental Laboratory, Seattle, Washington

ABSTRACT

A 14-yr time series of salinity at thermocline level was constructed from repeated meridional CTD sections (averaging about 110 days apart) spanning the equator along 165°E during 1984–97. A tongue of high salinity water extends along the isopycnal $\sigma_t = 24.5$ from its surface outcrop in the southeast Pacific to 175-m depth near 5°–10°S along the section at 165°E. In the west, the tongue moves vertically with the thermocline, mostly as part of the ENSO cycle, while salinity in the tongue varied interannually over a range of 0.4 psu. Most of this variability was due to zonal advection along the isopycnal tongue, with similar changes observed at other longitudes in the west and central Pacific. Part of the interannual salinity signal can be attributed to changes in the near-zonal flow of the South Equatorial Current associated with El Niño, but a general 0.3 psu rise occurring during the 1990s (probably starting even earlier) was not apparently consistent with this explanation. An attempt was made to trace the source of these changes to surface fluxes at the outcrop, where the variation of evaporation and precipitation suggested salinity anomalies of the same magnitude as the subsurface changes. However, the implied surface salinity changes were of the wrong sign to explain the subsequent downstream subsurface variability, and therefore present observations do not demonstrate any influence of subduction of surface properties on salinity in the southern high salinity tongue.

1. Introduction

Recent observational (Deser et al. 1996; Schneider et al. 1999), theoretical (McCreary and Lu 1994; Gu and Philander 1997), and modeling (Liu et al. 1994; Lysne et al. 1997; Rothstein et al. 1998) studies have suggested the importance of variations of the subtropical meridional overturning cells (STC) to the slow modulation of the equatorial Pacific. These cells advect water subducted in the downward-Ekman-pumping regions of the subtropical gyres along generally westward and equatorward geostrophic pathways on thermocline-level isopycnals. Because the North Pacific has historically been more densely instrumented, much of the observational focus has been there, but the equatorward pathways in the South Pacific are apparently much more direct, with larger property fluxes (Johnson and McPhaden 1999), due in part to the absence there of an Ekman upwelling region comparable to the ITCZ, which greatly complicates the situation in the north (Lu and McCreary 1995). However, despite the overall scantiness of subsurface ocean data in the South Pacific, in a few locations sufficient observations exist to construct time series that might show variations in the strength and properties of the South Pacific STC. The general paucity of salinity observations has restricted the STC observational focus to studies of temperature alone, but a few longitudes have seen repeated CTD sections that do resolve interannual subsurface salinity fluctuations, and the purpose of the present paper is to examine one such section, at 165°E, to determine the magnitude of the low-frequency thermocline-level salinity variations and investigate their causes.

A second motivation for the present work is the effect of salinity variations on the assimilation of temperature and satellite-altimeter-derived sea surface height variations into general circulation models for climate forecasting. Surface wind stresses alone are not sufficient to produce realistic model fields, so forecasting relies on a continuous input of realtime temperature profiles as a correction (Ji et al. 1995). Given the absence of real-time salinity data, density must be inferred from a mean temperature–salinity relation or regressions based on temperature profiles and satellite sea surface height (Ji and Leetmaa 1997). When salinity is strongly anomalous over a large enough vertical extent, these algorithms can produce erroneous density profiles and con-

---

Corresponding author address: William S. Kessler, NOAA/Pacific Marine Environmental Laboratory, 7600 Sand Point Way NE, Seattle WA 98115.
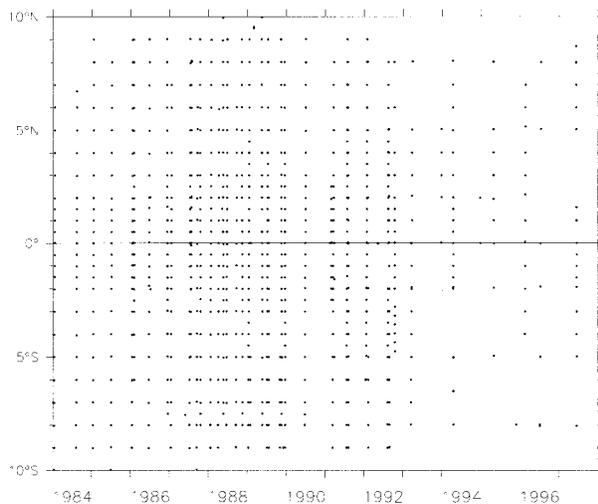E-mail: kessler@pmel.noaa.gov

FIG. 1. Location of profiles along 165°E, as a function of latitude and time. There were 917 profiles available on this section. Most of the profiles were taken in synoptic meridional sections (46 individual cruises).

sequent erroneous current fields. Such problems were noted in the course of forecasting the 1997–98 El Niño, in which model dynamic heights were too high by as much as 9 dyn cm over a wide region of the western equatorial Pacific, even with the assimilation of a substantial number of temperature profiles, due to the poor representation of the anomalously high salinity of 1996–97 (Ji et al. 1999; Vossepoel et al. 1999). Therefore it seems worthwhile from this point of view as well to learn more about the causes of thermocline-level changes in this dynamically active property.

2. Data collection and processing

a. CTD cruises along 165°E

Data used in this study are CTD profiles obtained from the NODC archives, with the addition of recent profiles made by the Pacific Marine Environmental Laboratory (PMEL). To construct the 165°E section, 917 profiles on 46 meridional cruise lines were available between 10°S and 10°N, 164° and 166°E, during the period 1984 through 1997 (Fig. 1). The 165°E section is one of the few places in the tropical Pacific where a multiyear time series of subsurface salinity data exists, as a result of several intensive international efforts to reoccupy the section during the 1980s. Semiannual cruises along 165°E were made out of Noumea, New Caledonia, by the ORSTOM laboratory there from 1984 through 1992, except 1990 (Delcroix et al. 1987). Other repeated cruises were made under the auspices of the U.S.–China program, by Japan Marine Science and Technology Center vessels, and by National Oceanic and Atmospheric Administration (NOAA) vessels in the course of deploying Tropical Atmosphere–Ocean moorings. Most of these cruises made CTD profiles to a 1000-

m depth at least every degree of latitude between 8°S and 8°N. Subsets of the 165°E sections have formed the basis for several previous studies of the circulation and properties in the western Pacific (Delcroix et al. 1987; Toole et al. 1988; Delcroix et al. 1992; Gouriou and Toole 1993)

Overall, the 46 cruises along 165°E averaged about 110 days apart over 14 years, but during the more intensely sampled periods in 1987–92 the average spacing was closer to 60 days (Fig. 1). However, very irregular cruise intervals meant that there were no years without at least a 3-month gap, and there were only two cruises in each of the years 1993–96 and one in 1997. We have no hope of resolving frequencies higher than annual, and even the annual cycle is barely evident in the time series.

For the purposes of estimating the zonal gradient of subsurface salinity and checking the representativeness of the 165°E time series, sections along 180° and 155°W were also constructed from the same CTD databases. There were 13 cruises along 180°, with 166 profiles, beginning in 1987. Most of these sections only extended from 5°S to 5°N, however. Along 155°W there were 13 cruises that made a total of 202 profiles, beginning in 1991.

The sparseness of the sampling, both in time and longitude, is a potentially serious source of error here where the aim is the estimation of the zonal advection of salinity. Some idea of the effect of temporal aliasing was obtained by subsampling the data from the period 1984–92, when the cruises were densest (Fig. 1). These cruises were sorted into two groups, and gridded fields of salinity and zonal geostrophic current recalculated from each subset by the methods described in sections 2b and 2c. A signal/noise (S/N) measure was the rms of fields from the full data divided by the rms of the difference due to subsampling. For the region 2°–8°S, the S/N was about 3 for salinity and about 1.5 for zonal current. This is borne out by statistics of the subsurface salinity variability seen during the relatively well-sampled (16 cruises in 18 months) Hawaii–Tahiti Shuttle experiment at 150°–158°W (Wyrtki and Kilonsky 1984). Salinity in the subsurface tongue during the Shuttle experiment showed fluctuations of 0.1–0.2 psu on timescales of 2–4 months, much of which would appear as aliasing under the sampling regime at 165°E. These crude tests indicate that the reduced sampling at 165°E during 1993–97 was near the minimum to adequately resolve the 0.3–0.4 psu interannual signals described here. No dense sampling was available to test the 15° longitude separation used here to estimate dS/dx.

b. Data gridding

One of the difficulties of working with sparsely sampled CTD sections is the aliasing as a water column heaves with internal waves at frequencies well above what is sampled by the cruises studied here. The vertical
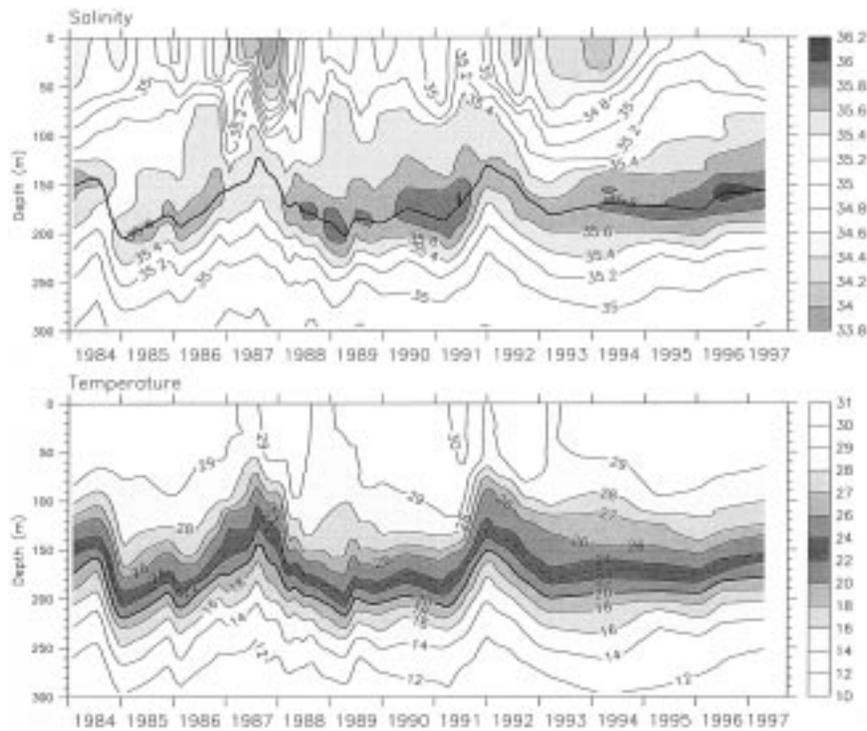
FIG. 2. Salinity (top) and temperature (bottom) at 3°–5°S, 165°E. The contour interval for salinity is 0.2 psu, and for temperature 2°C, with supplementary contours at 27° and 29°C. Shading indicates high salinity (top) and the central thermocline (bottom). The $\sigma_t = 24.5$ isopycnal is indicated by a thick line in the top panel and a dashed line in the bottom.

motion of the thermocline at 165°E that is unresolved by 100-day sampling has rms amplitude of 15–20 m (Kessler et al. 1996), which makes constructing time series of low-frequency phenomena at specific depths problematic, especially when comparing or taking derivatives between nearby locations contaminated by uncorrelated high-frequency internal wave variability. Such noise is seen in the jerkiness of the time series of Fig. 2, even given the 3° latitude averaging employed. However, since internal wave heaving is largely adiabatic, salinity on an isopycnal surface is much less aliased by vertical motion of the column than is salinity sampled at a particular depth. In this study, we take advantage of this property by studying variations of the salinity on the isopycnal $\sigma_t = 24.5$ (kg m^{-3}), which is close to the level of the salinity maximum (note the contour $\sigma_t = 24.5$ overlaid on the salinity mean section in Fig. 3 and the time series in Fig. 2). This isopycnal is found at a mean depth of about 175 m south of the equator along 165°E, and closely follows the 23°C isotherm in the upper thermocline. A salinity maximum was clearly seen in each profile, and these maxima were always found close to a density of $\sigma_t = 24.5$. Between 2° and 8°S the salinity maximum averaged about 2 m deeper than the isopycnal $\sigma_t = 24.5$, with an rms depth difference of about 5 m. Salinity on $\sigma_t = 24.5$ was found for each profile individually, then mapped to a monthly,

1° latitude grid by a two-dimensional Gaussian weighting procedure (Kessler and McCreary 1993) with e-folding scales of 6 months and 2° latitude. Figure 4 shows salinity on $\sigma_t = 24.5$ gridded in this manner as a function of latitude and time along 165°E. At 180° and 155°W, salinity on $\sigma_t = 24.5$ was found and gridded as described for 165°E (though these time series were shorter and sparser). At both locations, the depth of maximum salinity was within a few meters of the depth of the isopycnal $\sigma_t = 24.5$, as at 165°E.

c. Estimation of zonal geostrophic current on the isopycnal $\sigma_t = 24.5$

A common procedure to estimate the geostrophic zonal current on meridional sections is to find dynamic height relative to a deep reference as a function of latitude and depth and, from its meridional derivative, the full current field on each section, then selecting values at the desired depths. This method is used to find the mean zonal currents along 165°E shown in Fig. 3 (bottom). A disadvantage of this approach is that without heavy temporal smoothing, high-frequency noise is exacerbated by taking horizontal derivatives. Smoothing in latitude along the section, which might substitute for time smoothing, tends to reduce the speed of the narrow equatorial currents excessively. A more convenient
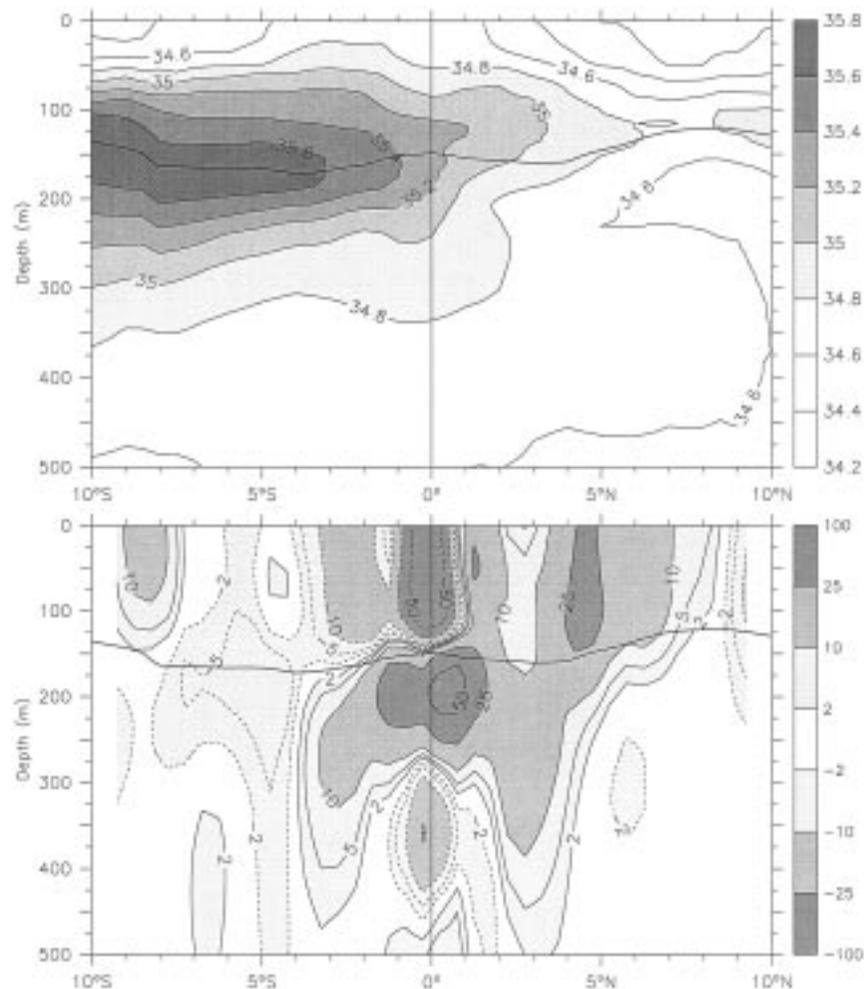
FIG. 3. Mean salinity (psu; top) and zonal geostrophic current relative to 700 m (cm s^{-1}; bottom) along 165°E. Shading indicates high salinity (top) and current speeds greater than 2 cm s^{-1}. The thick line overlaid on each panel is the mean depth of the $\sigma_t = 24.5$ isopycnal.

method for finding the geostrophic flow on an isopycnal directly was shown by Montgomery (1937), who derived an expression for streamlines of geostrophic currents on an isopycnal (strictly an isentropic) surface. Montgomery showed that on this surface the quantity $\psi = \alpha' P + \Phi'$, where α' is the specific volume anomaly, P the pressure, and Φ' the geopotential anomaly (dynamic height in dynamic meters times 10) is analogous to dynamic height, so that zonal and meridional geostrophic currents on the surface are $u_g = -\psi_y/f$ and $v_g = \psi_x/f$, where f is the Coriolis parameter. Contours of ψ are therefore streamlines of the geostrophic current on the isopycnal surface (but ψ is not a streamfunction because of the variation of f). Here, ψ is similar to what has been called the acceleration potential (Tsuchiya 1981; Tsuchiya et al. 1989). Use of ψ, even without any smoothing, reduces noise due to heaving of the column because if a column is stretched upwards, for example, the pressure on an isopycnal surface is smaller but the

dynamic height relative to an assumed motionless reference level is larger, so the internal wave noise tends to cancel. Contours of mean ψ are shown in Fig. 5 (discussed in section 3a) for the $\sigma_t = 24.5$ surface over the entire tropical Pacific using the Levitus et al. (1994) World Ocean atlas dataset. For the CTD profiles along 165°E studied here, values of ψ on $\sigma_t = 24.5$ were found at each profile and mapped as a function of latitude and time by the same Gaussian mapping procedure and scales as was done for the salinity, and then the meridional derivative of ψ was used to define the zonal geostrophic current on the isopycnal surface. The reference level for the geostrophic current was chosen at 700 m. For the off-equatorial currents of interest here, 700 m is below all significant shear, and this choice maximizes the number of usable profiles. For the equatorial currents, Gouriou and Toole (1993) compared geostrophic and measured zonal currents in the western equatorial Pacific (including an earlier subset of the data used here)
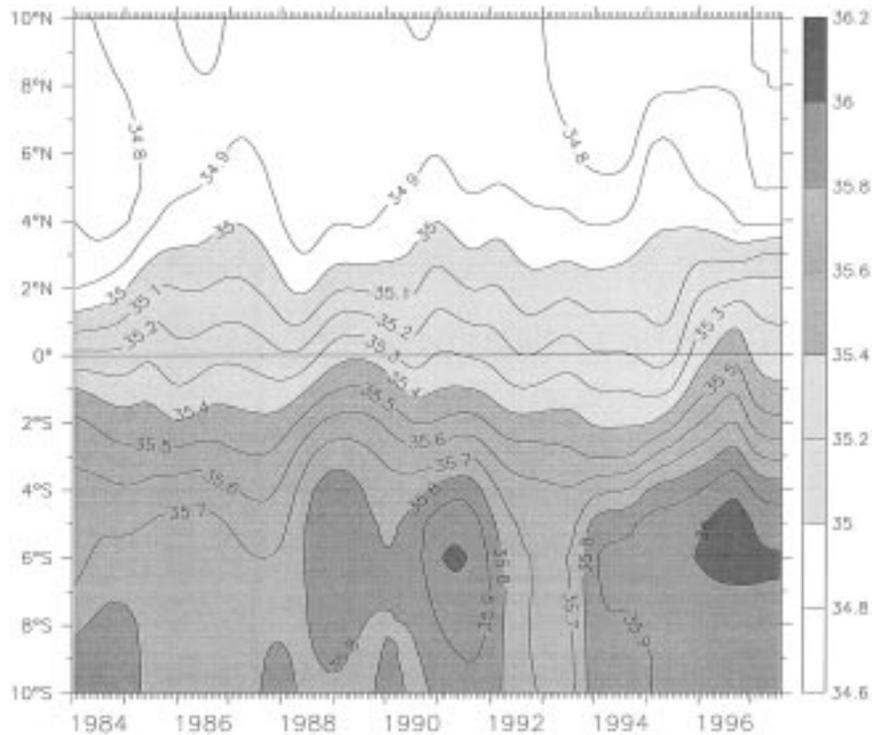
FIG. 4. Salinity on the isopycnal $\sigma_t = 24.5$ along 165°E as a function of latitude and time. The contour interval is 0.1 psu.

and found that a 600-m reference level gave the best agreement (but there is still shear at this level).

3. Results

Interannual variability of the depth of the salinity maximum south of the equator at 165°E consisted partly of vertical excursions over a range from about 140 to 190 m (Fig. 2), apparently associated with the ENSO cycle. The thermocline and salinity maximum were found at shallower depths during the El Niños of 1986–87 and 1991–92, consistent with the commonly observed shoaling of the west Pacific thermocline during warm events, as first suggested by Wyrtki (1975), and documented for the period 1975–89 by Delcroix and Henin (1989) and Donguy (1994). The shallow thermocline observed in 1984 was a long-lasting residual of the extremely strong shoaling associated with the 1982–83 El Niño (Kessler and Taft 1987). These three shallow-thermocline events extended over the entire 10°S–10°N meridional extent of the sections, and were not focused at the equator. During the 1994–95 warm event, expendable bathythermograph data indicates that the west Pacific thermocline shoaled relatively briefly and with less than half the amplitude of the earlier events (B. Kessler 1997, personal communication). South of the equator, the 1994–95 shoaling event was poorly sampled by the present set of CTD profiles (Fig. 1) and does not appear in Fig. 2.

The other aspect of variability of the salinity maximum, and the primary concern of the present work, is variability in the value of salinity near its maximum, on the isopycnal $\sigma_t = 24.5$. Figure 2 shows peaks of more saline water at 3°–5°S in 1984, 1988–89, 1990–91, and 1996. The latitude–time plot of salinity on ($\sigma_t = 24.5$ (Fig. 4) shows that these peaks were most intense near about 5°–6°S (except during 1984, when a high salinity peak was seen much farther south) and appeared with fresher water both to the south and north. Being maxima in the vertical, the high salinity values could not have been formed by any vertical processes at 165°E, and the fact that they represent meridional maxima as well (Fig. 4) shows that they also could not have come from meridional advective or diffusive events either. Therefore, we hypothesize that zonal advection was a likely source of this variability. To explore this idea, we first examine the zonal gradient of subsurface salinity, and then the geostrophic currents at 165°E.

a. The basinwide structure of the subsurface salinity maximum

The general pattern of mean salinity at thermocline level can be seen from the Levitus et al. (1994) World Ocean atlas (Fig. 5). Although the Levitus gridded dataset is rather highly smoothed, the picture described here is grossly in accord with fields carefully mapped along isopycnals recently produced by Johnson and
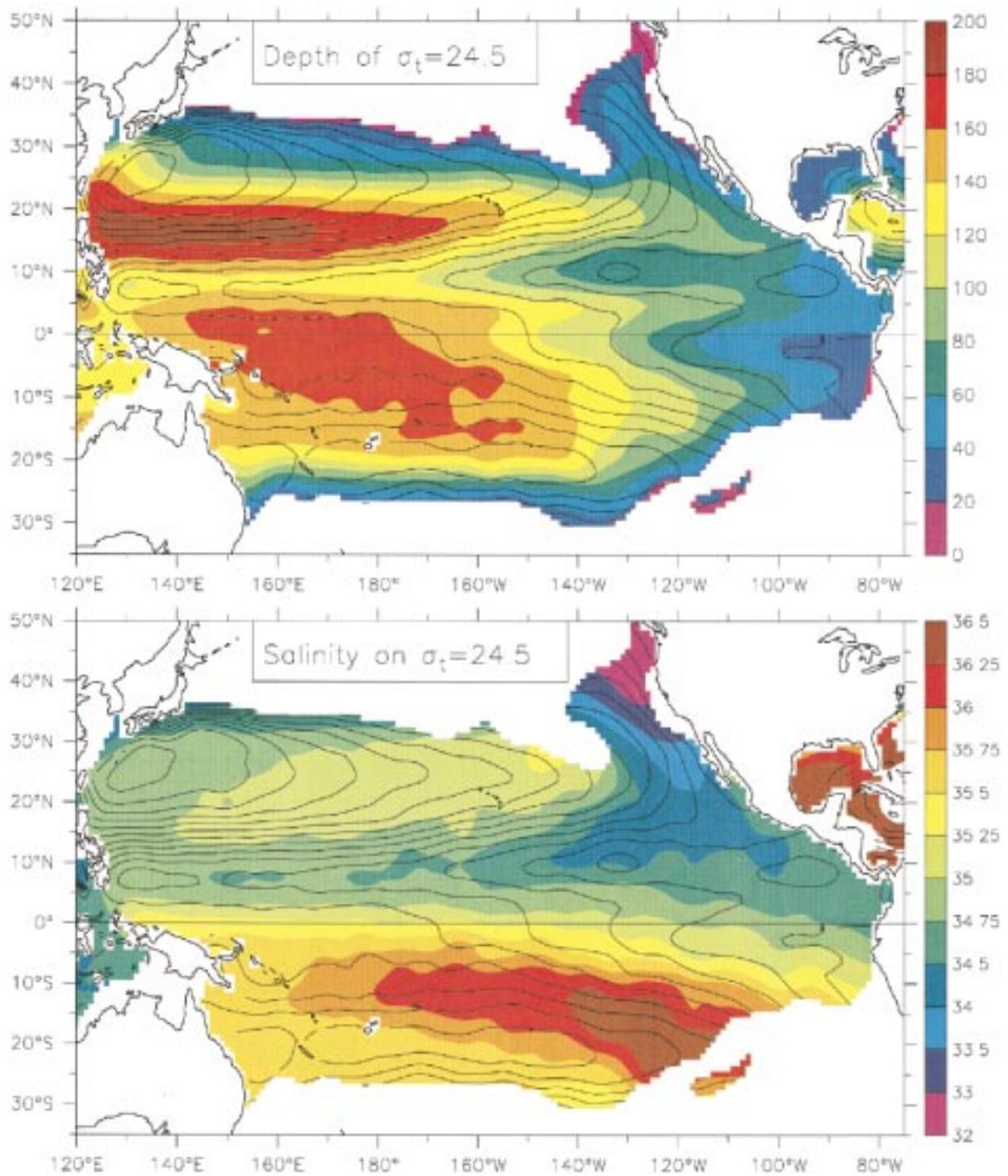
FIG. 5. Mean salinity and geostrophic streamlines on the surface $\sigma_t = 24.5$ from the Levitus et al. (1994) World Ocean Atlas. Top: Color shading indicates the depth of the $\sigma_t = 24.5$ surface (red = deeper). Bottom: Color shading indicates salinity on the $\sigma_t = 24.5$ surface (red = higher salinity). In both panels overlaid contours show the geostrophic streamlines on the surface relative to 1000 m. Flow is generally equatorward along these contours from ventilation regions at the poleward edges.

McPhaden (1999). The $\sigma_t = 24.5$ surface outcrops along about 25°S and 30°–35°N in the central and western Pacific, with a band extending farther north along the west coast of North America, but the cold, saline waters of the Humboldt Current (and coastal upwelling) along the South American coast push the 24.5 outcrop line almost to the equator there (Fig. 5). This isopycnal bowls down below 160 m over a broad region roughly under the west Pacific warm pool, ridges up to about 130 m along 8°N, and forms another deep bowl along about 15°N. Geostrophic flow on $\sigma_t = 24.5$ relative to 1000 m is indicated by the contours in Fig. 5, showing the northern and southern subtropical gyres, as well as other familiar features like the North Equatorial Countercurrent between about 2° and 8°N. In general, the isopycnal is ventilated from the eastern parts of the subtropical gyres along pathways that go westward and equatorward. Ventilation of the 165°E region south of the equator occurs roughly along the ψ contour that downwells from the surface near 15°–20°S, 110°W. Figure 5 shows that this flow path follows the north flank of a tongue of high salinity (and correspondingly high temperature, since this is an isopycnal), beginning with surface values of about 36.3 psu (virtually the highest mean surface salinity in the Pacific) and 24.5°C, becoming cooler and less saline along the path to values of about 35.8 psu and 23°C at 165°E, 170 m. This picture of the mean flow and properties along $\sigma_t = 24.5$ suggests that fluctuations of the zonal current at this level would result in significant salinity variability measured along the 165°E section. From Fig. 5, the mean zonal gradient of salinity at this level near 165°E is about 10^{-7} psu m^{-1}, so current variations of the order of 5–10 cm s^{-1} would be sufficient to produce the observed amplitude of interannual salinity variability (changes on the order of 0.2 psu yr^{-1}) seen in Fig. 4. It is also worth noting that in the region of the $\sigma_t = 24.5$ outcrop in the southeast Pacific the mean surface density gradient is very small, because surface temperature and salinity both fall to the southeast. More than 1000 km separate the mean latitudes of the $\sigma_t = 24$ and 25 surface isopycnals, about one-fifth the gradient observed in the central Pacific. Therefore small changes in the surface fluxes could also lead to potentially large changes in the location of the outcrop and the mix of properties subducted along the pathway.

b. Time variation of salinity and its zonal gradient

Figure 6 shows the time series of salinity on $\sigma_t = 24.5$ averaged over 3°–5°S at 165°E, 180°, and 155°W. While it would probably be preferable to study salinity advection closer to the meridional maximum (near 5°–6°S), sampling at 180° was confined largely north of 5°S, so this was not possible. However, salinity (and for the most part, zonal current) variability at $\sigma_t = 24.5$ along 165°E was coherent between about 2° and 8°S, so it is hoped that the results found here are relevant to
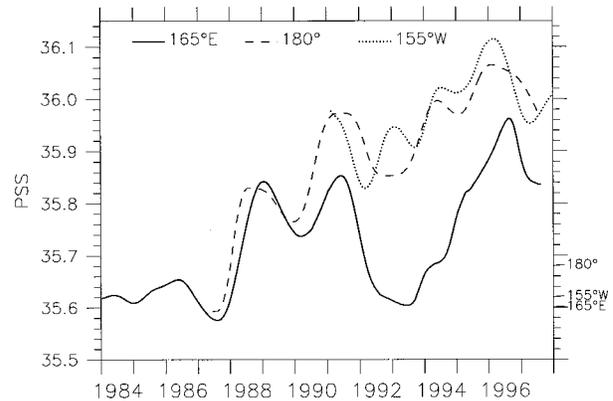

FIG. 6. Time series of salinity on $\sigma_t = 24.5$ at 3°–5°S along 165°E, 180°, and 155°W. Labelled ticks on the right axis indicate the mean values of salinity at each location from the Levitus et al. (1994) World Ocean Atlas.

the larger region. At all three locations salinity has generally increased by about 0.3 psu since the mid-1980s (this trend was similar at all latitudes between the equator and 8°S), with superimposed year-to-year variations of roughly 0.1 psu. (In none of these locations was it possible to resolve the annual cycle of subsurface salinity, but examination of salinity on $\sigma_t = 24.5$ during the 18-month-long Hawaii–Tahiti Shuttle suggests that the annual cycle at this level is small, less than 0.1 psu.) Although the sampling was coarse enough that one might have little confidence in details of the variability shown, the trend towards increasing salinity is clear. The fact that there is a good correspondence among the interannual peaks on three sections suggests that the depiction at this level of detail is realistic and also that these signals represent large-scale variability and are not due to eddy activity aliased by the crude time resolution.

These time series were used to estimate the variation of dS/dx between 165°E and 180° at 3°–5°S; ΔS varied between just below zero to about 0.3 psu, with a slow trend toward larger gradient during 1991 through 1994, with smaller gradient before and after (Fig. 7, top panel) Only the low-frequency variations of dS/dx can be studied with the present data, and it is not possible to evaluate whether more rapid changes in dS/dx affected the zonal advection of salt. In addition, the fact that the zonal derivative can only be evaluated from one side is a further disadvantage (however since the mean flow is westward, this is usually an upstream derivative and perhaps not such a bad choice for an advective calculation).

c. Zonal geostrophic currents at 165°E

Mean zonal currents over all 46 CTD sections along 165°E relative to 700 m are shown in Fig. 3 (bottom) (this is a mean over velocities calculated for each cruise separately, not velocity found from the mean temperature and salinity). The 0.5° latitude, 5-m vertical res-
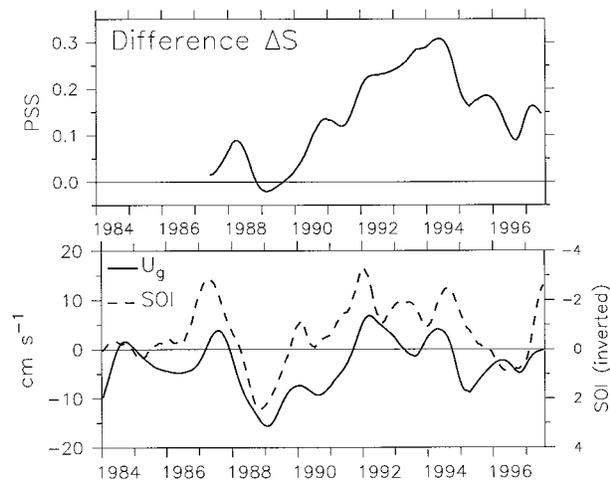
FIG. 7. Top: Salinity difference between 165°E and 180°, averaged between 3° and 5°S. Bottom: Zonal geostrophic current on the isopycnal $\sigma_t = 24.5$ along 165°E, averaged over 3°–5°S. The current on the isopycnal was calculated by the Montgomery (1937) method (see section 2c). The dotted line in the bottom panel is the Southern Oscillation Index inverted and divided by 2 (positive values indicate El Niño conditions).

olution used to make this section gives more detail than a corresponding section based on the Levitus compilation. Consistent with previous studies, given sufficient time-averaging even the equatorial currents can be determined geostrophically, except near the surface (Wyrtki and Kilonsky 1984; Lukas and Firing 1984; Delcroix et al. 1987; Gouriou and Toole 1993). The 165°E section shows the westward South Equatorial Current (SEC) near the surface from about 4°S to 1°N at speeds of up to 50 cm s^{-1}. South of the equatorial zone, the SEC is found at thermocline level with mean speeds of 2–6 cm s^{-1}. Below the SEC, the Equatorial Undercurrent (EUC) has maximum speed of 80 cm s^{-1} at a depth of 200 m. A westward Equatorial Intermediate current is below the EUC, and a fairly strong eastward current is below that [see Gouriou and Toole (1993) on the reference level for equatorial currents in the western Pacific]. The geostrophic North Equatorial Countercurrent reached peak eastward velocity of about 30 cm s^{-1} near 5°N, and the North and South Subsurface Countercurrents dangle from the flanks of the EUC. Above the SEC south of 4°S, the eastward South Equatorial Countercurrent (SECC) (Delcroix et al. 1987) was found in the upper 100 m. Mean speeds in this current were near zero between 4° and 6°S, as the surface current in this region is strongly variable, but a near-permanent surface SECC with mean speeds of 15 cm s^{-1} occurs near 8°S. The $\sigma_t = 24.5$ isopycnal and salinity maximum are found in the westward flow of the SEC at about 175 m depth, then pass just above the core of the EUC, as shown by the thick overlaid lines in Fig. 3. Mean zonal speed on the isopycnal was about 6 cm s^{-1} westward in the SEC near 5°S, decreasing to the north and south.

Time variability of zonal flow on $\sigma_t = 24.5$ at 3°–

5°S is shown in Fig. 7 (bottom panel), estimated on the isopycnal by the Montgomery (1937) method (see section 2c). The standard deviation of zonal current at this level was about 5 cm s^{-1} in the region 2°–8°S. Eastward flow regimes were seen during 1984–85, 1987, and 1992–94; this timing suggests a probable association with El Niño events, which is confirmed by the relatively good correlation between the observed current and the Southern Oscillation Index (SOI) of El Niño. The eastward flows occurred when the 24.5 isopycnal was at shallower levels, so it may be that it was a matter of lifting the isopycnal into the region of eastward flow in the SECC (Fig. 3, bottom); however, since changes in the isopycnal slope must be associated with geostrophic shear changes, such an interpretation is probably too simple. Without being able to resolve the time variability as a function of depth and latitude it is not possible to untangle this question. However, for the purposes of the present paper, the most important result from this zonal current time series is that periods of increasing salinity on the isopycnal south of the equator occurred in association with westward current maxima, that is, in 1984, 1988, 1990, and 1995–96 (Fig. 4), consistent with the hypothesis of advection along the high salinity tongue originating in the east.

d. Zonal advection of salinity at the level of the maximum

Multiplying the time series of dS/dx on the $\sigma_t = 24.5$ surface between 180° and 165°E (Fig. 7, top) with that of zonal current at 165°E (Fig. 7, bottom) gives the zonal advective contribution to salinity variability ($u\,dS/dx$) on $\sigma_t = 24.5$ at 3°–5°S, 165°E for the period 1987–96 (Fig. 8).

The comparison between $u\,dS/dx$ and dS/dt on $\sigma_t = 24.5$ shows that zonal advection was a significant influence on changes of salinity at this location (Fig. 8). The rms variability of dS/dt (0.012 psu month^{-1}) was about the same as that of $u\,dS/dx$, and the correlation was 0.59, which is significant at the 90% level (see the appendix). During 1987–96, two positive peaks show increasing salinity with a magnitude of $1–2 \times 10^{-2}$ psu month^{-1} on the isopycnal in 1988 and 1990–91, corresponding to salinity rises of about 0.1 psu. Salinity fell at a rate of greater than 2×10^{-2} psu month^{-1} during the latter half of 1991. A sustained (though bumpy) increase of about 1×10^{-2} psu month^{-1} was observed during 1993–96, corresponding to a net rise of more than 0.3 psu (Fig. 6). Salinity change due to zonal advection (dashed line in Fig. 8) had fair agreement with the total rate of change, as reflected in the significant correlation cited, and the phasing of the peaks and troughs was good [except for the more poorly sampled period 1994–96 (Fig. 1)]. Most of the phase variations and sign changes of $u\,dS/dx$ were due to variability of zonal currents, with one exception (discussed in the next paragraph).
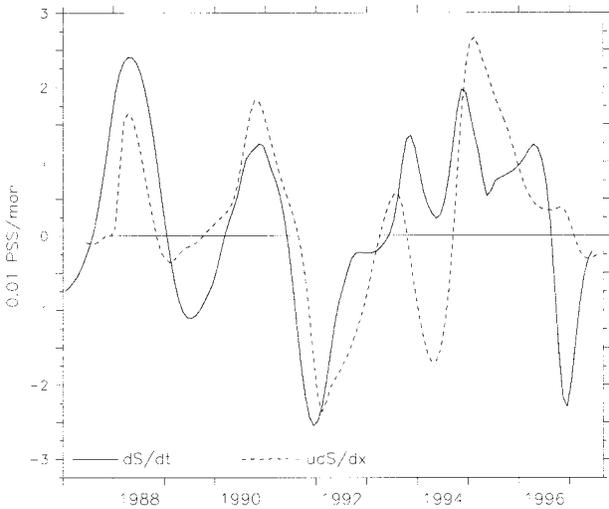
FIG. 8. Zonal advection of salinity on $\sigma_t = 24.5$ at 3°–5°S, 165°E, comparing dS/dt (line) and $u\,dS/dx$ (dash). Units are 0.01 psu month^{-1}.

Zonal advection was also estimated assuming a constant zonal salinity gradient, that is, $u\,\overline{dS/dx}$, where $\overline{dS/dx}$ is taken to be the average over the 1987–96 period. This neglect of the changes in zonal gradient degraded the comparison considerably, to a correlation of 0.32. The effect of the zonal gradient is to increase the magnitude of the zonal advective changes during 1991–95, and to reduce them before and after, and this aspect greatly improves the agreement. In addition, the sign change of $u\,dS/dx$ in 1988–89, which corresponds well to the observed salinity rate of change, is due to the sign change in dS/dx when salinity was greater at 165°E than at 180° (Fig. 6).

4. Discussion

High salinity at thermocline level in the western South Pacific extending toward the equator from the southern subtropical gyre is a manifestation of warm, saline water subducted in the southeast Pacific and advected west in the South Equatorial Current. A salinity maximum tongue is found on the isopycnal $\sigma_t = 24.5$, from an outcrop region near 15°–25°S, 110°W, along geostrophic streamlines to the 165°E section near 5°S at a depth of about 175 m (Fig. 5). Interannual variability of salinity along 165°E in this tongue during 1984–97 consisted of 1–2 yr fluctuations of order 0.1 psu, overlaid on lower-frequency signals that are two to three times larger, including a sustained rise of more than 0.3 psu that resulted in 1996 having the highest salinities of the previous 12 years on $\sigma_t = 24.5$ near 5°S on 165°E, 180°, and 155°W (Fig. 6). Variability of salinity on $\sigma_t = 24.5$ was at least 50% larger at 3°–7°S than on the rest of the section (Fig. 4). In addition, the entire thermocline–salinity maximum structure heaved vertically through a range of more than 50 m, apparently asso-

ciated with the ENSO cycle (Fig. 2). Although variability of salinity on $\sigma_t = 24.5$ at 165°E can appear as meridional motion toward and away from the equator, the occurrence of maxima isolated in depth and latitude and coherent in longitude suggests that zonal motion of the gyre-scale tongue is the cause. Estimation of zonal geostrophic currents of salinity based on repeated CTD sections at 165°E and 180° confirms that a large fraction of the salinity signal is associated with zonal advection, due both to changes in the zonal currents themselves and to the zonal gradient of salinity at the level of the maximum (Fig. 8). Considering that the high salinity tongue delineates a direct interior pathway from the subtropical subduction region to the equatorial undercurrent (Johnson and McPhaden 1999), it would be of great interest to establish the elements that control the variability of flow and properties of the tongue.

Variations of zonal currents on $\sigma_t = 24.5$ in the region of maximum salinity are due primarily to the ENSO cycle, with anomalously eastward currents during El Niño events (1987 and 1992–94 in this time series) and westward currents otherwise, particularly during the La Niña conditions of 1988 and 1995–96 (Fig. 7). The correlation between zonal geostrophic speed at 3°–5°S on $\sigma_t = 24.5$ and the SOI (smoothed by a 5-month running mean) was 0.7 for the period 1984–97. Since salinity usually increases eastward on $\sigma_t = 24.5$ (going up the tongue toward the outcrop), westward flow tends to raise the salinity and eastward flow to lower it. In the absence of other effects, one would therefore expect to see a decrease of salinity during El Niño events and an increase during La Niña conditions. Salinity on $\sigma_t = 24.5$ south of the equator did rise by 0.25 psu during the 1988 La Niña, and fell about the same amount during the 1991–92 El Niño. From 1987 through 1992, the zonal advective term matched the time rate of change of salinity better than in the latter part of the study period (Fig. 8), with a correlation of about 0.76 (compared to 0.59 for 1987–97). Contradicting this simple picture, however, between 1993 and 1996 salinity rose continuously to the highest values seen in the 13-yr record, even though 1993 was an (albeit weak) El Niño and 1994–95 was a strong one. Figure 8 shows that zonal advection acting alone would have postponed the rise until the end of 1994, which would be more consistent with an explanation in terms of the ENSO cycle [not surprising since the zonal currents followed this cycle fairly closely (Fig. 7)]. During this period the correlation between the time series of dS/dt and $u\,dS/dx$ was clearly worse (Fig. 8). These discrepancies may well be due to the paucity of observations south of the equator during 1993–96 (Fig. 1); in any case, there is not a satisfactory explanation at hand for the large rise of thermocline level salinity in the mid-1990s. The fact that a similar sustained salinity rise was observed on $\sigma_t = 24.5$ at the other meridional sections studied (180° and 155°W; Fig. 6), indicates that a very large scale process was at work.

An attempt was made to look back up the geostrophic

streamline (Fig. 5, bottom) along the high salinity tongue on $\sigma_t = 24.5$ to trace changes back to the outcrop near 15°–20°S, 110°W. The mean speed along the geostrophic streamline found from the Levitus et al. (1994) World Ocean atlas data is about 10 cm s^{-1}, which would imply a lag of about one-half year from 165°E to 180°, 1.5 years to 155°W, and 3 years to the outcrop region near 110°W. The three times series (Fig. 6) do not show such lags clearly, although the time resolution is poor and it is possible that the lag exists (recent modeling studies (Liu et al. 1994; Gu and Philander 1997) suggest longer lags of up to ten years). Therefore it is worth estimating the changes in mixed-layer properties near the outcrop to see if this provides clues to the salinity changes at 165°E.

Since there is only extremely sporadic salinity data (or in fact any ocean data) in the outcrop region [see Delcroix and Henin (1991) and Delcroix et al. (1996) for surface salinity observations and variability in nearby regions], surface salinity was deduced entirely from an estimation of changes in precipitation and evaporation as follows. Monthly rainfall on a 2.5° latitude–longitude grid was estimated from an index derived from the microwave sounding unit satellite precipitation (Spencer 1993) for the period 1979–96. Precipitation in the outcrop region averaged about 5 cm month^{-1}; its 12-month running mean ranged from 3 to 7 cm month^{-1}. Evaporation was estimated from bulk aerodynamic formulae using SST, air temperature, and wind speed from the European Centre for Medium-Range Weather Forecasts (ECMWF) 12-hourly analysis based on real-time assimilation for 1985–97. In the absence of any data, a constant relative humidity of 75% was assumed. Evaporation averaged about 14 cm month^{-1} with variability somewhat smaller than that for precipitation and not correlated with it. The outcrop region therefore showed a net mean evaporation in the outcrop region amounting to about 9 cm month^{-1}, with annual average fluctuations on a roughly 5–8-yr timescale of about 4 cm month^{-1}. To estimate salinity changes due to precipitation minus evaporation $(P - E)$, a 50 m thick instantly mixed surface layer was assumed, with its initial value the Levitus et al. (1994) mean surface salinity. Each month of the common period of January 1985 through December 1996, the net anomalies from the 12-yr mean of $P - E$ were added to (or subtracted from) the mixed layer as fresh water and the resulting salinity integrated forward. The mixed layer salinity time series, averaged over the region 130°–110°W, 25°–15°S, deduced from this procedure remained near the initial value of about 36.2 psu from 1985 through 1991, then fell to about 35.7 psu until 1996 before rising again to about 35.9 psu. As pointed out in section 3a, the surface density gradient in this region is very small because both surface salinity and temperature fall to the southeast, so the location of the outcrop can change by hundreds of kilometers with even small surface density changes. Therefore, the time series of deduced surface salinity

as a function of space and time was combined with the Reynolds and Smith (1994) satellite-derived SST to construct fields of surface density, and salinity along the (time varying) position of the $\sigma_t = 24.5$ outcrop was extracted. During the early 1990s, the entire region appeared to warm and freshen slightly (about 0.2°C and 0.5 psu), pushing the surface isopycnal toward the cooler and fresher region to the south. Although the position of the outcrop varied substantially during this period (from 20° to 28°S at 110°W), the deduced surface salinity was very similar to the area-averaged time series.

Assuming a 3-yr lag from the outcrop to 165°E, the 0.5 psu estimated surface salinity freshening during the early 1990s was of the wrong sign to explain the features of observed salinity on $\sigma_t = 24.5$ at the three interior locations (155°W, 180°, and 165°E), in which the most prominent feature was a sustained increase of salinity on this isopycnal at the time when the assumed fresher subducted water would be arriving. No adjustment of the expected geostrophic speed could improve the comparison, since rising surface salinity at the outcrop (which would be necessary if the observed salinity downstream was to be attributed to subducted surface changes) was not inferred until 1996, after the increase at 165°E. Obviously the estimate based on surface fluxes alone is crude and subject to great uncertainty, yet there appears to be no other way of evaluating changes at the outcrop. It must be concluded that no evidence can be adduced here to support a hypothesis that variability at the outcrop region influenced subsequent changes of subsurface salinity downstream.

5. Summary

Time series of subsurface salinity and density south of the equator were constructed from an essentially complete CTD profile database for the period 1984–97. The 165°E section is one of the few places in the tropical Pacific where decade-long time series are well enough resolved by historical data to depict interannual subsurface salinity variability. A tongue of high salinity extending westward and equatorward from a ventilation region in the southeast Pacific is one limb of a subtropical cell connecting subtropical subduction to the equator at thermocline level. Interannual variability of salinity in the tongue consisted of year-to-year peaks with magnitude typically 0.1–0.2 psu, strongly influenced by advection along the tongue in the South Equatorial Current. For much of the period, variability of this advection was due in large part to zonal current fluctuations associated with the ENSO cycle, especially a 0.2 psu rise during the La Niña of 1988 and a corresponding freshening during the El Niño of 1991–92. However, an apparent long-term trend (a 0.3 psu rise) over the length of the 14-yr time series was seen at 165°E, with similar increases in the shorter time series at 180° and 155°W, and this could not be easily explained in terms of ENSO cycle currents.

Theory and modeling studies suggest that changes in the properties of water subducted in the subtropical gyres should be advected along isopycnals westward and equatorward. Although determining variability of surface fluxes in the ventilation region in the southeast Pacific is limited by the lack of observations, an attempt to estimate these fluxes and infer mixed layer salinity indicated interannual changes of similar magnitude to those observed downstream at three longitudes athwart the isopycnal pathway. However, the sign of the inferred subducted variability was opposite to what would be needed if the downstream salinity changes were be accounted for by variations at the isopycnal outcrop, and no adjustment of the assumed advection speed could bring these into even rough balance. Since the surface flux calculation here is very crude, it cannot be said with certainty that variations of subduction did not influence salinity along the pathway, but present observations do not demonstrate such any influence in the Southern Hemisphere high salinity tongue.

APPENDIX

Significance of Cited Correlations

A correlation coefficient r, with n_f degrees of freedom, may be transformed to a variable z, approximately normally distributed with standard deviation σ_z (Panofsky and Brier 1968)

$$z = \frac{1}{2} \ln\left(\frac{1+r}{1-r}\right); \qquad \sigma_z = \frac{1}{\sqrt{n_f - 3}}. \quad \text{(A1)}$$

This transformation, together with its inverse $r = \tanh(z)$, is commonly used in constructing confidence intervals for the correlation coefficient. The number of degrees of freedom n_f associated with each correlation value was obtained by dividing the number of cross product terms (common months for the two monthly time series) by the independence timescale (Davis 1976)

$$\tau_{ij} = \Delta t \sum_k C_{ii}(k\Delta t) C_{jj}(k\Delta t), \quad \text{(A2)}$$

where the subscripts i and j refer to the two time series correlated, and $C_{ii}(k\Delta t)$ is the autocorrelation of time

series i for lag $k\Delta t$. Since z is normally distributed, Eq. (A1) and a table of the t test (e.g., Panofsky and Brier 1968, their Table 14) then give the 90% confidence range $z \pm 1.645 \, \sigma_z$, which is inverted back to the 90% confidence range on the correlation coefficient r.

For the time series of dS/dt and $u\,dS/dx$ shown in Fig. 8, the independence timescale (A2) was found to be about 10 months, and for 127 common months of observation (1987 through mid-1997) this gives about 12 degrees of freedom. The 90% confidence range on r is about ± 0.50, and the correlation coefficient cited in section 3d (0.59) is significantly different from zero at the 90% level.

REFERENCES

Davis, R. E., 1976: Predictability of sea surface temperature and sea level pressure anomalies over the North Pacific Ocean. *J. Phys. Oceanogr.,* **6,** 249–266.

Delcroix, T., and C. Henin, 1989: Mechanisms of subsurface thermal structure and sea surface thermohaline variabilities in the southwestern tropical Pacific during 1975–85. *J. Mar. Res.,* **47,** 777–812.

——, and ——, 1991: Seasonal and interannual variations of sea surface salinity in the tropical Pacific Ocean. *J. Geophys. Res.,* **96,** 22 135–22 150.

——, G. Eldin, and C. Henin, 1987: Upper ocean water masses and transports in the western tropical Pacific. *J. Phys. Oceanogr.,* **17,** 2248–2262.

——, ——, M. H. Radenac, J. M. Toole, and E. Firing, 1992: Variation of the western Pacific Ocean. *J. Geophys. Res.,* **97,** 5423–5445.

——, C. Henin, V. Porte, and P. Arkin, 1996: Precipitation and sea surface salinity in the tropical Pacific Ocean. *Deep-Sea Res.,* **43,** 1123–1141.

Deser, C., M. A. Alexander, and M. S. Timlin, 1996: Upper ocean thermal variations in the North Pacific during 1970–1991. *J. Climate,* **9,** 1840–1855.

Donguy, J.-R., 1994: Surface and subsurface salinity in the tropical Pacific Ocean: Relations with climate. *Progress in Oceanography,* Vol. 34, Pergamon Press, 45–78.

Gouriou, Y., and J. Toole, 1993: Mean circulation of the upper layers of the western equatorial Pacific Ocean. *J. Geophys. Res.,* **98,** 22 495–22 520.

Gu, D., and S. G. H. Philander, 1997: Interdecadal climate fluctuations that depend on exchanges between the Tropics and extratropics. *Science,* **275,** 805–807.

Ji, M., and A. Leetmaa, 1997: Impact of data assimilation on ocean initialization and El Niño prediction. *Mon. Wea. Rev.,* **125,** 742–753.

——, ——, and J. Derber, 1995: An ocean analysis system for seasonal to interannual climate studies. *Mon. Wea. Rev.,* **123,** 460–481.

——, R. W. Reynolds, and D. Behringer, 1999: Use of TOPEX/Poseidon sea level data for ocean analyses and ENSO prediction: Some early results. *J. Climate,* in press.

Johnson, G., and M. J. McPhaden, 1999: Interior pycnocline flow from the subtropical to the equatorial Pacific Ocean. *J. Phys. Oceanogr.,* in press.

Kessler, W. S., and B. A. Taft, 1987: Dynamic heights and zonal geostrophic transports in the central tropical Pacific during 1979–84. *J. Phys. Oceanogr.,* **17,** 97–122.

——, and J. P. McCreary, 1993: The annual wind-driven Rossby wave in the subthermocline equatorial Pacific. *J. Phys. Oceanogr.,* **23,** 1192–1207.

——, M. C. Spillane, M. J. McPhaden, and D. E. Harrison, 1996:

Scales of variability in the equatorial Pacific inferred from the TAO buoy array. *J. Climate,* **9,** 2999–3024.

Levitus, S., R. Burgett, and T. P. Boyer, 1994: *World Ocean Atlas 1994,* Vol. 3: *Salinity.* NOAA/NESDIS/NODC, 99 pp.

Liu, Z., S. G. H. Philander, and R. C. Pacanowski, 1994: A GCM study of tropical–subtropical upper-ocean water exchange. *J. Phys. Oceanogr.,* **24,** 2606–2623.

Lu, P., and J. P. McCreary, 1995: Influence of the ITCZ on the flow of thermocline water from the subtropical to the equatorial Pacific Ocean. *J. Phys. Oceanogr.,* **25,** 3076–3088.

Lukas, R., and E. Firing, 1984: The geostrophic balance of the Pacific equatorial undercurrent. *Deep-Sea Res.,* **31,** 61–66.

Lysne, J., P. Chang, and B. Giese, 1997: Impact of the extratropical Pacific on equatorial variability. *Geophys. Res. Lett.,* **24,** 2589–2592.

McCreary, J. P., and P. Lu, 1994: On the interaction between the subtropical and equatorial oceans: The subtropical cell. *J. Phys. Oceanogr.,* **24,** 466–497.

Montgomery, R. B., 1937: A suggested method for representing gradient flow in isentropic surfaces. *Bull. Amer. Meteor. Soc.,* **18,** 210–212.

Panofsky, H. A., and G. W. Brier, 1968: *Some Applications of Statistics to Meteorology.* University of Pennsylvania Press, 224 pp.

Reynolds, R. W., and T. M. Smith, 1994: Improved sea surface temperature analyses using optimum interpolation. *J. Climate,* **7,** 929–948.

Rothstein, L. M., R.-H. Zhang, A. J. Busalacchi, and D. Chen, 1998: A numerical simulation of the mean water pathways in the subtropical and tropical Pacific Ocean. *J. Phys. Oceanogr.,* **28,** 322–342.

Schneider, N, A. J. Miller, M. A. Alexander, and C. Deser, 1999: Subduction of decadal North Pacific temperature anomalies: Observations and dynamics. *J. Phys. Oceanogr.,* **29,** 1056–1070.

Spencer, R. W., 1993: Global ocean precipitation from the MSU during 1979–91 and comparisons to other climatologies. *J. Climate,* **6,** 1301–1326.

Toole, J. M., E. Zou, and R. C. Millard, 1988: On the circulation of the upper waters in the western equatorial Pacific Ocean. *Deep-Sea Res.,* **35,** 1451–1482.

Tsuchiya, M., 1981: The origin of the Pacific equatorial 13°C water. *J. Phys. Oceanogr.,* **11,** 794–812.

——, R. Lukas, R. A. Fine, E. Firing, and E. Lindstrom, 1989: Source waters of the Pacific equatorial undercurrent. *Progress in Oceanography,* Vol. 23, Pergamon Press, 101–147.

Vossepoel, F. C., R. W. Reynolds, and L. Miller, 1999: Use of sea level observations to estimate salinity variability in the tropical Pacific. *J. Atmos. Oceanic. Technol.,* in press.

Wyrtki, K., 1975: El Niño—The dynamic response of the equatorial Pacific Ocean to atmospheric forcing. *J. Phys. Oceanogr.,* **5,** 572–584.

——, and B. Kilonsky, 1984: Mean water and current structure during the Hawaii-to-Tahiti Shuttle Experiment. *J. Phys. Oceanogr.,* **14,** 242–254.